Vol. **135** (2019) *ACTA PHYSICA POLONICA A* No. 3

Using the Spin–Orbit Coupling for Studying the Structural, Elastic, Electronic, Ferromagnetic, and Thermoelectric Properties of the Ti_2PdX (X = Al, Ga, and In) Full-Heusler Alloy Compounds

A. Boudali[a,*], A. Mokaddem[b], B. Doumi[a] and H. Moujri[c]
[a]Laboratory of Physico-Chemical Studies, University of Saida, Algeria
[b]Centre Universitaire Nour Bachir El Bayadh, 32000, Algeria
[c]LPMMAT, Faculty of Sciences Ain-Chock, Hassan II University, Casablanca, Morocco

(Received May 19, 2018; in final form January 5, 2019)

We have presented in this paper a systematic study predictive of the physical elastic constants, thermoelectric properties, correction of the gap, and the polarization by the application of spin–orbit coupling on Ti_2PdX compounds (X = Al, Ga, and In) using first principles quantum mechanics calculations. The structural optimization was performed using generalized gradient approximation and spin–orbit coupling within full potential linear augmented plane wave method. The alloys are found to be ferromagnetic semi-metallic in the Hg2CuTi structure-type with a total magnetic moment per unit cell equal to 3.00 μ_B. The stability is assessed from the physical point of view. The half-metallicity is conserved when varying the lattice constant from 5.8 to 7.0 Å. The compounds obey the Slater rule $Mt = Zt - 24$. The thermoelectric performance of our compounds are done by combining the results of *ab initio* band-structure calculations and the Boltzmann transport theory in the framework of the constant relaxation time (τ) approximations as incorporated in BoltzTraP code.

DOI: 10.12693/APhysPolA.135.409

PACS/topics: full-Heusler compound, thermoelectric properties, magnetic and electronic properties, half-metallic character, electrical conductivity

1. Introduction

German mining engineer and chemist Friedrich Heusler was the first to study such alloys in 1903. These alloys contain two proportions of copper, a proportion of manganese and a proportion of tin, which give Cu2MnSn and having the following properties. Its magnetism varies considerably with heat and composition [1]. They were found to have room-temperature saturation induction of about 8000 Gs, which is higher than that of nickel (about 6100 Gs), but smaller than that of iron (about 21500 Gs). First studies, out by Bradley and Rogers [2–4] in 1934, showed that the ferromagnetic phase at room temperature corresponded to a totally ordered $L21$ structure [5]. This structure (Cu2MnAl) is characterized by a cubic primitive lattice consisting of copper atoms with meshes centered alternately by manganese and aluminum atoms with a lattice parameter of 5.95 Å. The molten alloy has a solidification temperature of about 910 °C. When cooled below this temperature, it is transformed to the beta cubic centered disordered solid phase. Below 750 °C, a $B2$ ordered lattice is formed with a primitive cubic lattice of copper atoms which is centered by a disordered sub-lattice of manganese and aluminum atoms [6]. Cooling below 610 °C induces, moreover, order of the sub-lattice of manganese and aluminum to $L21$ structure [7]. In non-stoichiometric alloys, order temperatures decrease and the temperature range of annealing, where the alloy does not form micro-precipitates, becomes smaller than that of the stoichiometric material [1, 8]. Oxley found a value of 357 °C for the Curie temperature, below which the alloy is ferromagnetic [9]. Neutron diffraction and other techniques have shown that a magnetic moment of about 3.7 μ_B lies almost exclusively on manganese atoms [10]. Since these atoms are separated by 4.2 Å, the exchange interaction, which aligns the spins, is probably indirect and occurs via the conduction electrons or the aluminum and copper atoms [9, 11]. Electron microscopic studies have shown that thermal antiphase boundaries (APBs) form during cooling through order temperatures, since the ordered domains nucleate in different centers within the crystal lattice and are often in phase where it meet [6]. The anti-phase domain increases when the alloy is annealed. There are two types of APBs corresponding to the $B2$ and $L21$ order types. APBs also form between the dislocations if the alloy is deformed. At the thermal anti-phase boundaries (APB), the manganese atoms are closer than the mass of the alloy and, for non-stoichiometric alloys with an excess of copper (e.g. $Cu_{2.2}MnAl_{0.8}$), an antiferromagnetic layer forms on each thermal APB [12]. These antiferromagnetic layers completely replace the normal structure of the magnetic domain and remain with the APBs if they

---

*corresponding author; e-mail: abdelkader.boudali54@gmail.com grow by annealing the alloy. This substantially modifies the magnetic properties of the non-stoichiometric alloy with respect to the stoichiometric alloy which has a normal domain structure. This phenomenon is probably related to the fact that pure manganese is antiferromagnetic although it is not clear why the effect was not observed in the stoichiometric alloy.

Similar effects occur at APBs in the ferromagnetic alloy MnAl in the stoichiometric composition [13, 14]. Another useful (interesting) Heusler alloy is the class of materials known as ferromagnetic shape memory alloys. These are generally composed of nickel, manganese, and gallium and can change their length by up to 10% in a magnetic field [15–17].

Electronics was a huge development in the last three decades, but little attention has been given to the inclusion of magnetic materials in integrated electronic devices [18, 19]. However, a new field of electronics and spintronics has attracted widespread attention recently. In the spintronic context, both the spins and the electrical charge of electrons are controlled in the information transfer operation in the circuits [20, 21].

For a long time, magnetic materials and semiconductors have been developed separately with magnetic materials mainly used for data storage such as in hard disc drives in processors. It is a major challenge to integrate the two classes of materials for the development of spintronics devices.

Spintronics devices combine the advantages of magnetic materials and semiconductors to be multilateral, fast and non-volatile. Currently, technological and industrial advances in various fields are highly dependent on the advancement of research in the magnetic materials field (new characteristics of materials must be taken into account: spin polarization, conduction band, polarized carrier symmetry, the magnetism of the interfaces, etc.) [22–24].

One of the spintronics applications is the use of half-metals. One of the main properties of these materials is "half-metallicity", that is, the conduction electrons are 99.2% spin-polarized due to a deviation at the Fermi level [25]. This phenomenon stimulates a great interest in the development of materials that possess this property; a new class was predicted called ferromagnetic half-metals. A promising class of these materials is the Heusler alloys and more precisely that of the Mn-based ferrimagnetic Heusler alloys which has received considerable attention in theoretical studies [26–30].

In this work, we study the alloys Ti_2PdX (X = Al, Ga, and In) which is not yet synthesized. The study is carried out using *ab initio* simulation, within the framework of the density functional theory (DFT), at which we propose to perform the structural, electronic, and magnetic properties. In addition, we present the theoretical study of transport properties (of the compounds studied) calculated using the Boltzmann theory implemented in the BoltzTrap code [31]. In this work, we studied the structural, elastic, electronic, and magnetic properties of the same materials studied by Berri et al. [32], but with the spin–orbit coupling correction that is necessary for the Pd, our results in particular the gaps and the polarization are much better improved compared to the results of Berri et al. [32]. In addition, we have studied the elastic and thermoelectric properties of the same materials that have not been studied before to our knowledge.

2. Calculation method

We have calculated the structural, elastic, electronic, magnetic, and thermoelectric properties of the full Heusler alloy Ti_2PdX (X = Al, Ga, and In) by using the first principle theory based on the full-potential, linearized augmented plane wave method [33] in the framework of the DFT [34, 35] as implemented in the code WIEN2k [36]. The exchange and correlation energy is treated by the generalized gradient approximation (GGA) [37] and the Boltzmann transport equation under the constant relaxation time approximation (RTA) [38–40], for charge carriers as implemented in the BoltzTrap code [31]. Wave functions, electronic densities, and potential are expanded in the basis of spherical harmonics around atomic sites in muffin-tin spheres with a cut-off $\ell_{max} = 12$, while in the interstitial region, the set of basic function are taken as the Fourier series with a cut-off $R_{MT}K_{\max} = 8$ (where R_{MT} is the radius of the muffin-tin sphere and K_{max} is maximum wave vector for the basis set of plane waves). Within this predictive calculation, it has been shown that our studied compounds are ferromagnetic, with a total moment $M_t = 3.00\ \mu_B$. As we know, in *ab initio* calculations the crystal structure is very necessary to predict the physical properties of such material.

Our compounds belong to full Heusler family X2YZ which crystallizes in the cubic phase of space group No. 225 (Fm-$3m$) or No. 216 (F-$43m$) whose atomic positions are shown in Fig. 1a and b. With an accuracy on the order of 10^{-4} Ry, the structural properties are achieved by sampling of the Brillouin zone grid ($14 \times 14 \times 14$) with 120 special k-points in the first Brillouin zone. The used muffin-tin radii R_{MT}, of the constituent elements of the studied compounds, are reported in Table I. The cutoff energy, which defines the separation between the core and valence states, is set to -6.0 Ry. The relativistic effects are taken into account by the use of the scalar relativistic approximation to calculate the electronic states. For the electronic and magnetic calculations of the cubic Heuslers Ti_2PdX (X=Al, Ga, and In), we calculate the total and partial densities of states as well as the band structure along different directions of high symmetry using a grid ($14 \times 14 \times 14$) with 120 special points corresponding to 3000 k-points in the first Brillouin zone. As stated above, we used GGA approximation instead of local-spin-density approximation (LSDA) since GGA gives more accurate results, especially for electronic properties, but unfortunately it underestimates the gap [41], typically by 30 to 50%,

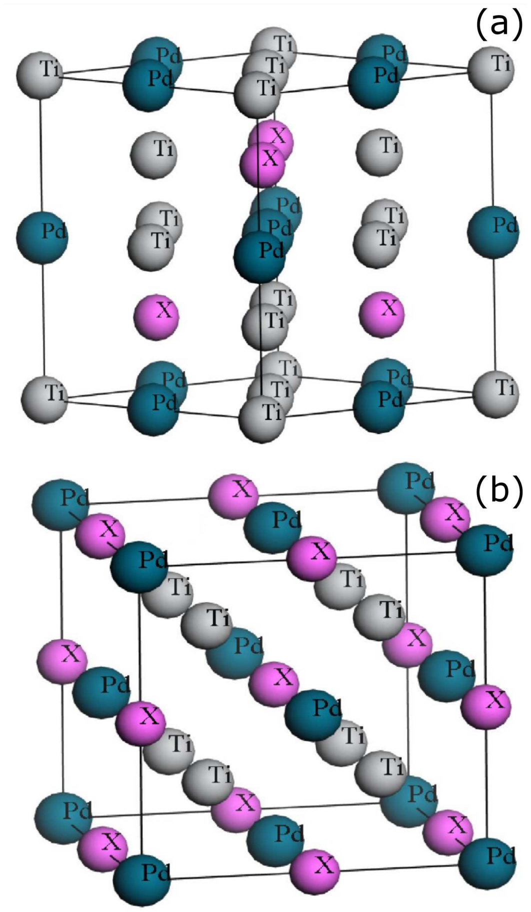

Fig. 1. Atomic positions of Ti_2PdX (X = Al, Ga, and In): (a) $CuHg_2Mn$-type $L2_1$ structure Ti(1) (0, 0, 0), Ti(2) (1/4, 1/4, 1/4), Pd(1/2, 1/2, 1/2), and X (3/4, 3/4, 3/4), (b) $CuHg_2Mn$-type $L2_1$ structure Ti (1/4, 1/4, 1/4), Pd (0, 0, 0) and X (1/2,1/2, 1/2).

without affecting the other electronic properties. This is due to the fact that the exchange and exact-correlation potentials, which are unknown, are discontinuous when the system goes from N to $N \pm 1$ particles [42, 43], because DFT does not have an equivalent of Koopmans' theorem for the Hartree–Fock method to calculate $E(N) - E(N \pm 1)$ where E is the total energy of the system [44]. This discontinuity of potential also exists for hybrid functional systems (B3LYP, B3PW, etc.), based in part on an exact exchange potential of the Hartree–Fock type. But hybrid functional systems give gaps more comparable to the experimental gaps than those provided by LDA or GGA, through moving the whole conduction band to the valence band. Some authors solve this problem by using an operator scissors; this amounts to moving toward the higher energies of the calculated conduction states by a quantity equal to the difference between the experimental gap and the calculated gap. For our part, we preferred to present our results as they were obtained. Calculations are performed taking into account the semi-core states due to the important overlap between these states and the valence states. For the band structure calculations, the equilibrium lattice parameter of each studied material is estimated. The space group of our materials Ti_2PdX (X = Al, Ga, and In) is Fm-$3m$. As mentioned above, relativistic scalar approximation is used for heavy atoms which have important electronic charge. Finally, the spin–orbit coupling is not considered since it affects slightly the results.

TABLE I

Muffin-tin radius R_{MT} of the elements constituting Ti_2PdAl, Ti_2PdGa and Ti_2PdIn.

Alloys	R_{MT} [Å]			
	Ti(1)	Ti(2)	Pd	X
Ti_2PdAl	2.31	2.31	2.46	2.20
Ti_2PdGa	2.25	2.25	2.46	2.25
Ti_2PdIn	2.37	2.37	2.46	2.43

3. Results and discussions

3.1. Structural properties

Figure 1a and b illustrates the two possible structures in which the full-Heusler alloys X2YZ crystallize: the $CuHg_2Ti$ structure-type and the Cu_2MnAl structure-type. All our calculations are realized for the most stable phase which can be found by performing structural optimization of both FM and PM phases of Ti_2PdX (X = Al, Ga, and In) in $CuHg_2Ti$ and Cu_2MnAl structure-type. The optimization consists in calculating the total energy as a function of the volume of the unit cell. After fitting the total energy to the equation of state of Murnaghan [45], the obtained results are presented in Fig. 2a and b where it can be clearly deduced that for all the studied compounds, the FM phase is the most stable with significantly smaller equilibrium energy than that of the PM phase.

The equilibrium energy of the two both phases are also determined and are listed in Table II. The formation energy indicates the stability of the alloys in regard of decomposition into its bulk constituents. The formation energy is calculated using the formula

$$E_f = E^{total}_{Ti_2PdX} - (2E^{bulk}_{Ti} + E^{bulk}_{Pd} + E^{bulk}_{X})$$

where E^{bulk}_{Ti}, E^{bulk}_{Pd} and E^{bulk}_{X} (X = Al, Ga, and In), correspond to the total energy per atom for Ti, Pd, and X atoms, respectively, obtained by the same approximation

TABLE II

Representation of the total energy of the magnetic phase No. 225 (Fm-$3m$) Cu_2MnAl structure-type (A) and the magnetic phase No. 216 (F-$43m$) $CuHg_2Ti$ structure-type (B).

Phase structure-type	Equilibrium energy [Ry]		
	Ti_2PdAl	Ti_2PdGa	Ti_2PdIn
A	−13985.507518	−17386.127261	−25262.064291
B	−13985.536274	−17386.160584	−25262.084925

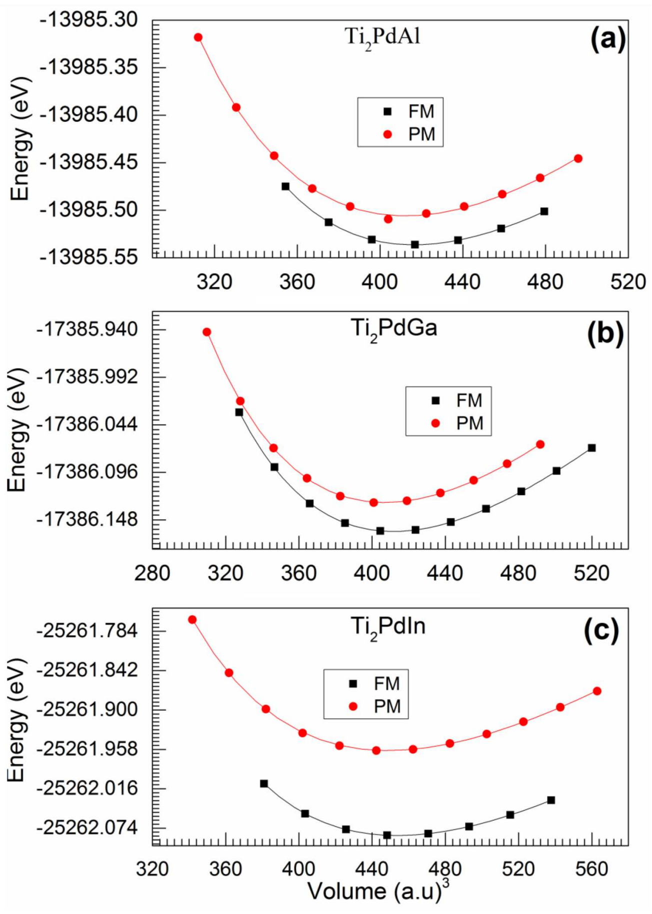

Fig. 2. Calculated total energy vs. the unit cell volume for the full-Heusler compound $\mathrm{Ti_2PdX}$ (X = Al, Ga, and In) with $\mathrm{Hg_2CuTi}$-type structure for FM.

used in the calculation of $E^{total}_{\mathrm{Ti_2}PdX}$. We found that the calculated formation energies are −1.66, −1.56, and −1.47 Ry for $\mathrm{Ti_2PdAl}$, $\mathrm{Ti_2PdGa}$, and $\mathrm{Ti_2PdIn}$, respectively, which indicates that the $\mathrm{Ti_2PdX}$ (X=Al, Ga, and In) alloys are thermodynamically stable due to their negative formation energies.

3.2. Elastic properties

It is well known that for cubic materials, three independent elastic constants are needed to describe the crystal elasticity: C_{11}, C_{12}, and C_{44}. The elastic constants C_{11} and C_{12} are obtained by application of a stress tensor with the orthorhombic volume retained. For the elastic constant C_{44}, a monoclinic stress tensor with a conserved volume is used.

Another important elastic property is the elastic anisotropy of a crystal which is evaluated by the so-called the anisotropy factor. The former provides information about eventual microcracks or other structural defaults appearing during the crystal growth process. The anisotropy factor A unity for isotropic materials [46], is the usual anisotropy factor given by

$$A = \frac{2C_{44}}{C_{11} - C_{12}}. \tag{2}$$

The elastic anisotropy A^* is given by [47]:

$$A^* = \frac{3\,(A-1)^2}{3\,(A-1)^2 + 25A}. \tag{3}$$

A^* have the following properties of practical importance:

1. A^* is zero for the crystals of the elastic isotropy, i.e., $A = 1$.
2. For an anisotropic crystal, A^* is a single-valued measure of the elastic anisotropy regardless of whether $A < 1$ or $A > 1$.
3. A^* gives a relative magnitude of the actual elastic anisotropy possessed by a crystal.
4. The difference $(A-1)$, whether positive or negative, is a measure of the degree of elastic anisotropy of the material.

The calculated structural and elastic properties for $\mathrm{Ti_2PdX}$ (X = Al, Ga, and In) compounds are summarized in Table III with no experimental or other theoretical data. The conditions of mechanical stability for cubic crystals should verify the obtained results of the elastic constant and the bulk modulus: $C_{11} - C_{12} > 0$, $C_{11} > 0$, $C_{44} > 0$, $C_{11} + 2C_{12} > 0$, $C_{12} < B < C_{11}$ [48, 49]. The obtained results show that the FP-LAPW method is an appropriate and efficient manner to investigate structural and elastic properties.

TABLE III

Structural and elastic properties of $\mathrm{Ti_2PdX}$ (X = Al, Ga, and In) full Heusler: a — lattice constant, B_0 — bulk modulus, B_0' — pressure derivative bulk modulus, C_{11}, C_{12}, and C_{44} — elastic constants, A — factor of elastic anisotropy.

Parameters	$\mathrm{Ti_2PdAl}$	$\mathrm{Ti_2PdGa}$	$\mathrm{Ti_2PdIn}$
a [Å]	6.2519	6.2235	6.4327
B_0 [GPa]	140.4613	142.6656	134.8059
B_0'	4.9116	4.5764	4.9345
C_{11} [GPa]	168.34255	193.85925	181.12660
C_{12} [GPa]	57.70325	126.45000	124.08065
C_{44} [GPa]	129.00050	55.95840	102.20975
A	2.331910994	1.660258792	3.583418279
A^*	0.250958007	0.091639371	0.548013516

4. Electronic and magnetic properties

The plots of the spin-up and spin-down band structure of $\mathrm{Ti_2PdX}$ (X = Al, Ga, and In) full Heusler compounds are presented in Fig. 3a–f. The band structures of our compounds are similar in shape; all these compounds exhibit a metallic behavior for the spin-up band structure, since the conduction and valence bands overlap at the level Fermi, while an indirect gap $\Gamma - X$ is observed near

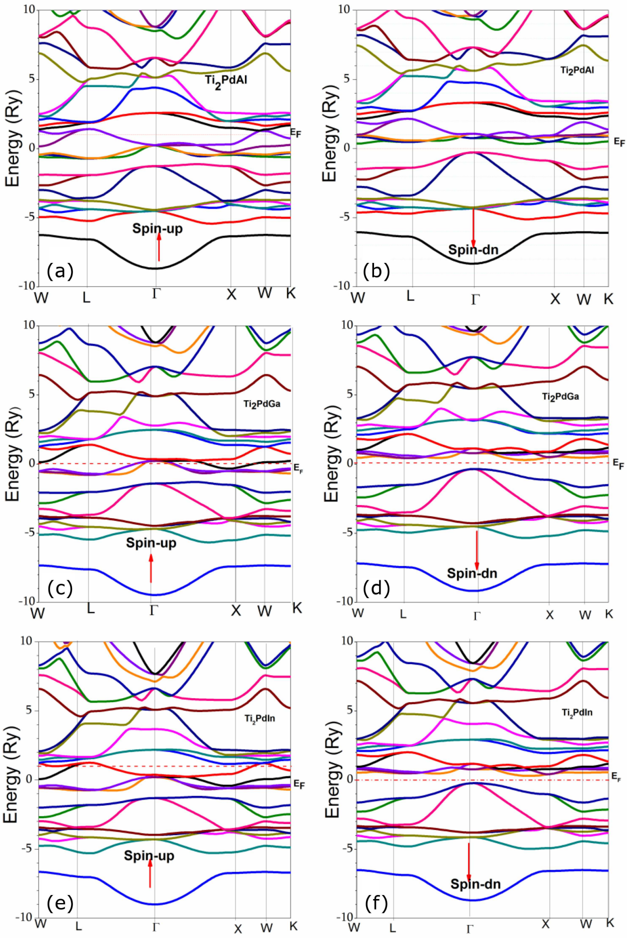

Fig. 3. Band structures spin-up and spin-down of the Ti$_2$PdX (X = Al, Ga, and In).

the Fermi level for the spin-down band structure indicating a semiconductor character of these compounds. Thus, the Ti$_2$PdX (X = Al, Ga, and In) compounds are half-metallic.

To elucidate the band structures, we calculated the partial and total densities of states for spin-up and spin-down of Ti$_2$PdX (X= Al, Ga, and In) compounds at equilibrium lattice constant. The representative curves of PDOS and DOS are shown in Figs. 4, 5, and 6. The calculated total magnetic moment for Ti$_2$PdX (X = Al, Ga and In) compounds is 3.00 μ_{B} which agree with the Slater–Pauling rule $Mt = Zt - 24$ and with the atomic magnetic moment of Ti(1), Ti(2), Pd, Al, Ga, and In. The effective magnetic moments, optimized energy are tabulated in Table IV. The spin-up channel exhibits a metallic character of the compounds since the DOS intersects EF, while the spin-down channel shows a semiconductor nature with a weak indirect gap $\Gamma \rightarrow X$ of 0.45, 0.50, and 0.45 eV without spin–orbit coupling, while with spin–orbit coupling the gaps are 0.44, 0.49, and 0.35 around the Fermi level for Ti$_2$PdX (X = Al, Ga, and In), respectively. This behavior leads to 99.1%, 99.3%, and 99.4% carrier spin polarization at EF, giving rise to half-metallic ferrimagnet compounds. From Figs. 4, 5, and 6 we observe in spin-down group that the strongly hybridized Pd–d and Ti(1)–d and Ti (2), states mainly contribute in the valence band around the Fermi level with sharp peaks at (6.06, 0.69, and 0.80 eV), (5.89, 0.54, and 0.58 eV) and (7.60, 0.45, and 0.53 eV) for Ti$_2$PdAl, Ti$_2$PdGa, and Ti$_2$PdIn respectively. In spin-down channel, the conduction band is essentially composed of d states of Ti atoms. In this region, peaks were observed at (6.66 and 7.11 eV), (4.86 and 6.50 eV) and (5.73 and 7.85 eV), for Ti$_2$PdAl, Ti$_2$PdGa, and Ti$_2$PdIn, respectively. The DOS of Ti(1) and Ti(2) atoms is situated principally above the Fermi level, in between −9 and −7 eV and consists mainly of s states of X atoms.

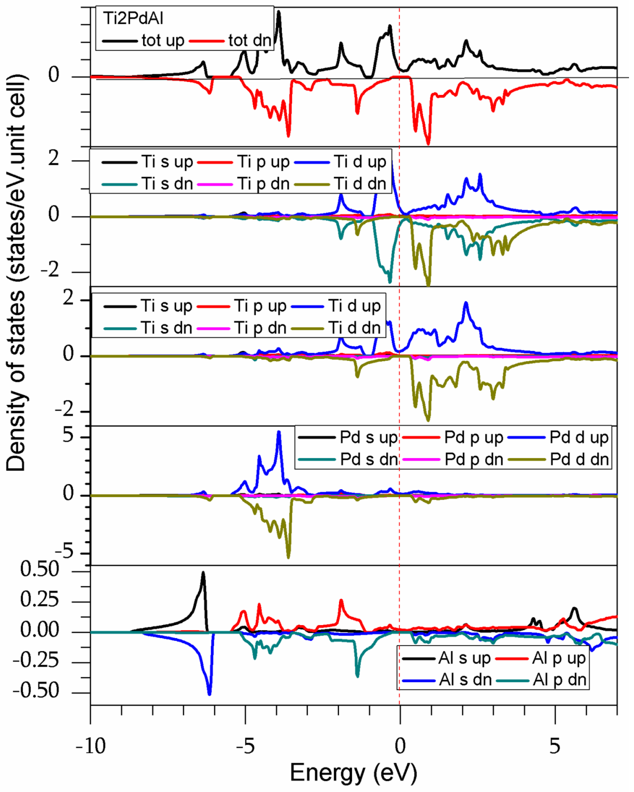

Fig. 4. Total and partial states of density for both spin-up and spin-down of Ti$_2$PdAl.

To study the effect of the lattice parameter on the half-metallicity, we performed electronic structure of Ti$_2$PdAl, Ti$_2$PdGa and Ti$_2$PdIn lattice parameter of 6.2519, 6.2235, and 6.4327 Å. From Table III, one sees that, when increasing the lattice constant, the Fermi level moves toward the conduction band and move to the valence band by decreasing the lattice constant. Therefore the half-metallic nature of Ti$_2$PdX (X = Al, Ga, and In) is conserved under compression or expansion. Figure 5 shows the magnetic moments of the Ti(1), Ti(2) and Pd atoms as a function of the lattice constant. Local moments can undergo important changes, but the total moment remains constant and equals 3.00 μ_{B}, since E_f stays within the gap.

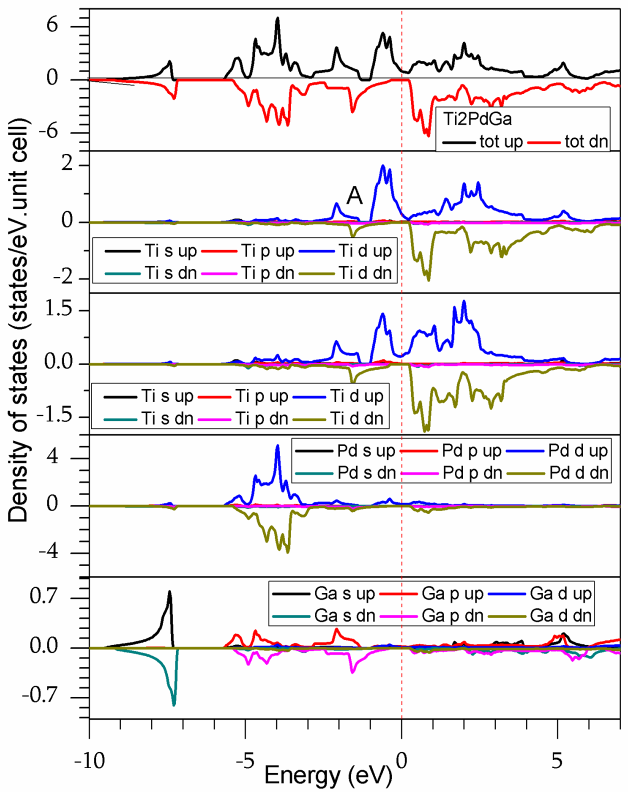

Fig. 5. As in Fig. 4, but for Ti_2PdGa.

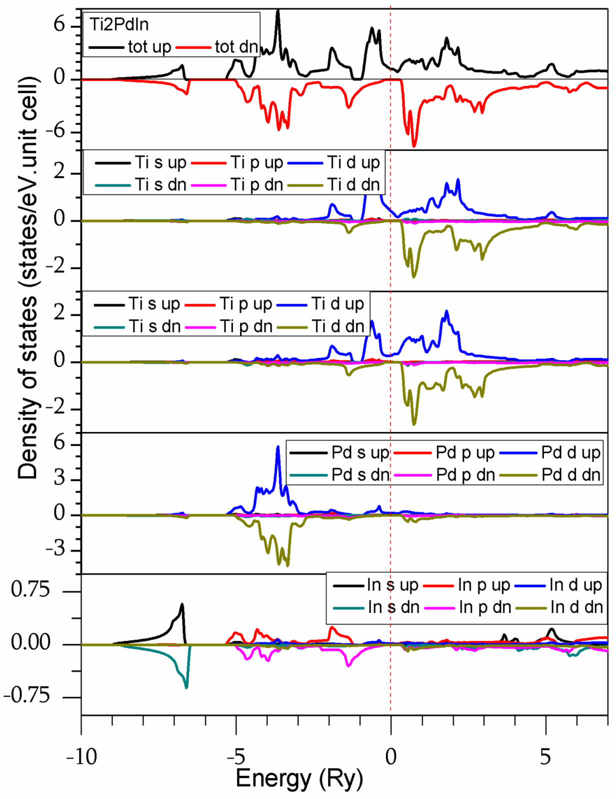

Fig. 6. As in Fig. 4, but for Ti_2PdIn.

TABLE IV

Total and partial magnetic moments of Ti_2PdX (X = Al, Ga, and In) Heusler compounds at equilibrium, and indirect gap around Fermi level.

Compounds	$\mu_{\text{interstitial}}$ [μ_B]	μ_{1Ti} [μ_B]	μ_{2Ti} [μ_B]	μ_{Pd} [μ_B]	μ_X [μ_B]	μ_{tot} [μ_B]	E_g [eV]
Ti_2PdAl	0.55312	1.44316	0.90727	0.09432	0.00250	3.00037	0.45
Ti_2PdGa	0.56176	1.40008	0.92193	0.11475	0.00191	3.00043	0.50
Ti_2PdIn	0.54329	1.40011	0.93773	0.10909	0.01055	3.00077	0.45

5. Thermoelectric properties

5.1. Thermoelectric properties as a function of the chemical potential

To our knowledge, this is the first study to investigate the thermoelectric properties of Ti_2PdAl, Ti_2PdGa, and Ti_2PdIn full Heusler compounds. The performance of a thermoelectric material can be predicted by the value of its figure of merit (ZT), which is related to the Seebeck coefficient, the electrical conductivity and the thermal conductivity by the relationship $ZT = \sigma S2T/\kappa$, where S is the Seebeck coefficient, σ is the electrical conductivity, T is the temperature and κ is the thermal conductivity. It is established that materials having ZT greater or equal to unity are considered as excellent candidates for thermoelectric applications [50, 51]. Figure 6a–c shows the variation of ZT with respect to the chemical potential of Ti_2PdA1, Ti_2PdGa, and Ti_2PdIn, respectively. ZT shows approximately the same behavior for these materials. For all compounds, ZT is clearly very close to the unity at room temperature. ZT increases sharply with the chemical potential and it reaches the maximum values at chemical potentials of -0.1 and 0.1 μeV to which correspond maximum values of the Seebeck coefficient and minimum ones of the thermal conductivity. Beyond these points, ZT decreases rapidly due to the sharp increase of the thermal conductivity.

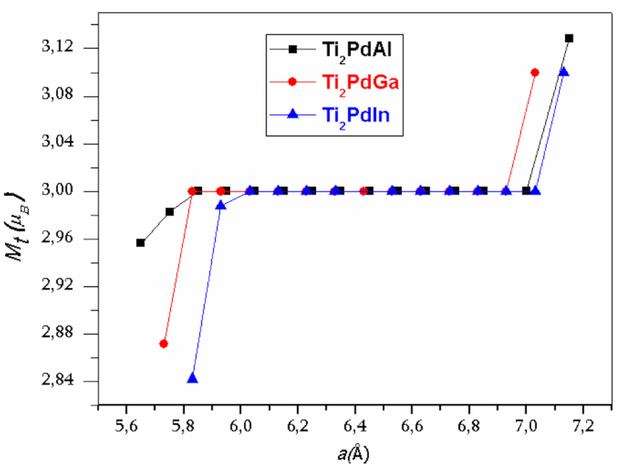

Fig. 7. The domain of half-metallic of Ti_2PdX.

Figure 7a–c illustrates the variation of the Seebeck coefficient of the studied materials Ti_2PdAl, Ti_2PdGa, and Ti_2PdIn respectively, as function of the chemical potential at temperatures of 300, 600, and 800 K. We note that the Seebeck coefficient has the maximum values of 953.5, 1014, and 855 μV/K at room temperature for Ti_2PdAl, Ti_2PdGa, and Ti_2PdIn compounds, respectively. This indicates that our compounds are good thermoelectric materials. The chemical potential values which separate the p and n-types materials are 0.12, 0.02, and 0.11 for Ti_2PdAl, Ti_2PdGa, and Ti_2PdIn, respectively. The Seebeck coefficient curve is characterized by the existence of two peaks in the chemical potential $(-1.0, 0.5)$, $(-1, 0.2)$ and $(-1.0, 0.25)$ μeV, for Ti_2PdAl, Ti_2PdGa, and Ti_2PdIn compounds, respectively, while beyond these ranges, the Seebeck coefficient vanishes rapidly. However, we expect that the compounds Ti_2PdAl, Ti_2PdGa, and Ti_2PdIn have good thermoelectric properties in their chemical potential ranges.

The electrical conductivity relative (σ/τ) of the Ti_2PdAl, Ti_2PdGa, and Ti_2PdIn compounds is calculated as function of chemical potential. The obtained results are displayed in Fig. 8a–c. We can see obviously that the electrical conductivity has the same feature at temperatures 300, 600, and 800 K for all compounds. The electrical conductivity is almost zero in the chemical potential ranges of $(-0.24, 0.30)$, $(-0.3, 0.3)$ and $(-0.23, 0.27)$ μeV for Ti_2PdAl, Ti_2PdGa, and Ti_2PdIn compounds, respectively. These ranges are all located in the middle of the chemical potential domains, mentioned above where the two Seebeck peaks are located, for all studied compounds. For p-type materials, the electrical conductivity reaches its maximum values at the chemical potential values of -1.26, -1.40, and -1.31 for Ti_2PdAl, Ti_2PdGa, and Ti_2PdIn respectively, at 300 K, whereas for n-type ones, the maximum electrical conductivity values are found at 1.48, 1.49, and 1.37 for Ti_2PdAl, Ti_2PdGa, and Ti_2PdIn, respectively. At these chemical potential energies, for both n and p-type materials, we observe that the electrical conductivity decreases with the increase of temperature.

The electronic thermal conductivity κ/τ versus the chemical potential is calculated independent of the relaxation time τ by mean of the BoltzTraP code. Figure 9a–c depicts thermal conductivity versus chemical potential for the Ti_2PdAl, Ti_2PdGa, and Ti_2PdIn compounds, respectively. From these figures, we can observe that the electronic thermal conductivity increases with respect to the temperature. The obtained value of the electronic thermal conductivity for Ti_2PdAl, Ti_2PdGa, and Ti_2PdIn compounds is about 75×10^{14} W/(m K) at 800 K.

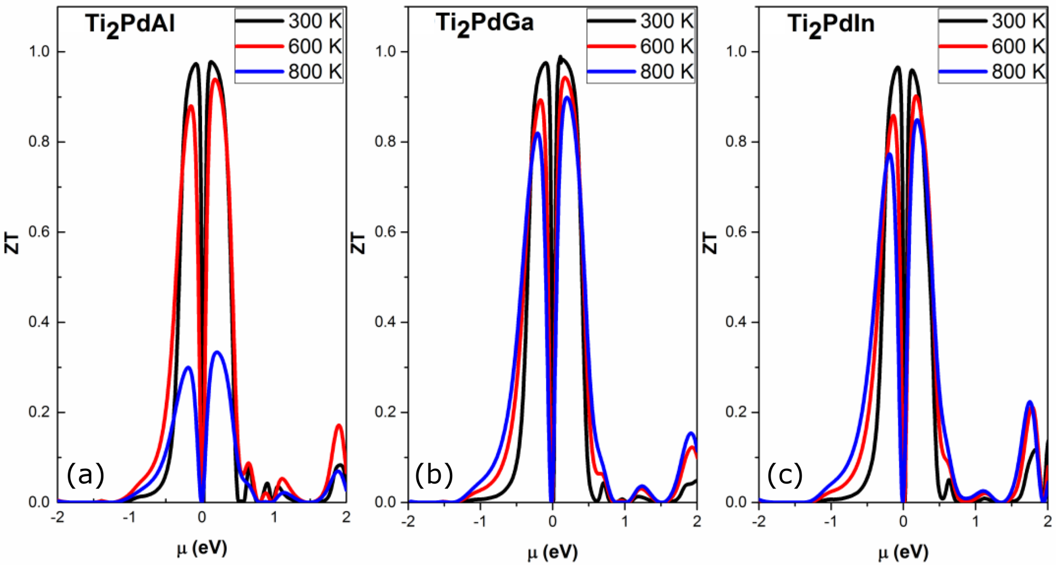

Fig. 8. ZT vs. chemical potential for Ti_2PdX.

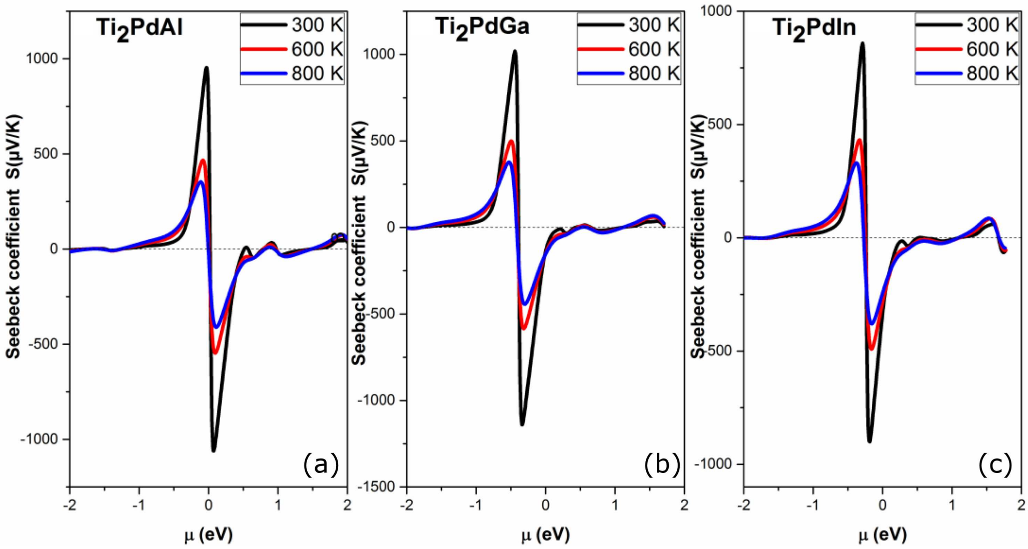

Fig. 9. Seebeck coefficients for (a) Ti_2PdAl, (b) Ti_2PdGa and (c) Ti_2PdIn at 300, 600 and 800 K.

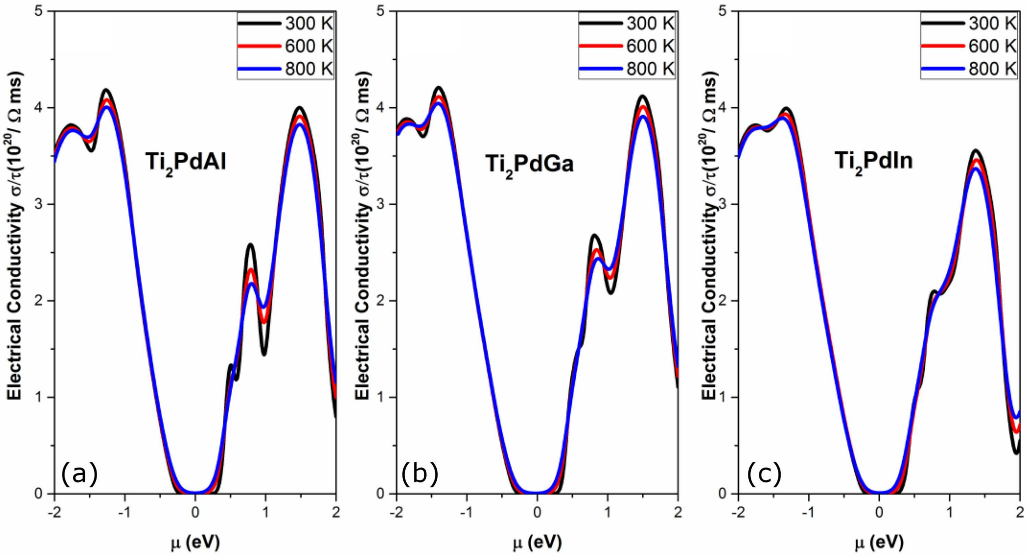

Fig. 10. Electrical conductivities of Ti_2PdX as a function of chemical potential at 300, 600, and 800 K.

5.2. Thermoelectric properties as a function of the temperature

To study the thermoelectric properties of the full-Heusler compounds Ti_2PdX (X = Al, Ga, and In), we used the Boltzmann semi-classical transport theory, based on the Fourier bands interpolation, implemented in the BoltzTraP code. The Seebeck coefficient S, the electrical conductivity σ/τ and the thermal conductivity (κ/τ) are calculated as a function of temperature (at $E_F = E_{F0}$, E_{F0} is the Fermi energy at $T = 0$ K for the studied compounds. We have predicted above that our studied compounds are magnetic materials, so we can use the two-stream model [52, 53] in which the Seebeck coefficient can be expressed as

$$S = \{[S(\uparrow) \times \sigma(\uparrow) + S(\downarrow) \times \sigma(\downarrow)] / [\sigma(\uparrow) + \sigma(\downarrow)]\},$$

where $S\sigma(\uparrow)$ and $\sigma(\downarrow)$ are the Seebeck coefficients and the electrical conductivity respectively for both spin-up $(\uparrow)$ and spin down $(\downarrow)$. In addition, it is important to note that the value of S for semiconductors is about 100 times greater than that of metals [54]. It is known that the studied compounds Ti_2PdX (X = Al, Ga, and In) are not pure semiconductors, but they exhibit a half-metallic behavior. In the following, we will consider only the spin-down states witch correspond to the semiconductor character of the materials. The Seebeck coefficient, which connects thermal and electrical conductivity, is an important thermoelectric property to estimate thermoelectric performances [55] of materials.

Figure 10 shows the temperature dependence of the thermoelectric coefficients of the full-Heusler compounds Ti_2PdAl, Ti_2PdGa, and Ti_2PdIn for the spin down states. It is seen that the absolute values of the Seebeck coefficient of the three compounds increase with the decrease of the temperature. Among the three studied compounds, Ti_2PdAl shows the highest Seebeck coefficient

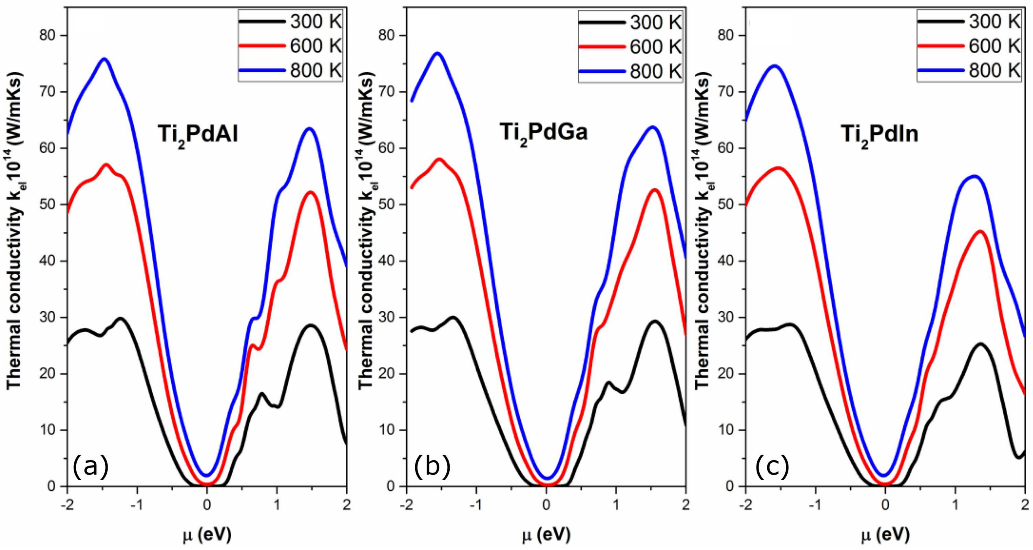

Fig. 11. Thermal conductivities of Ti_2PdX as a function of chemical potential.

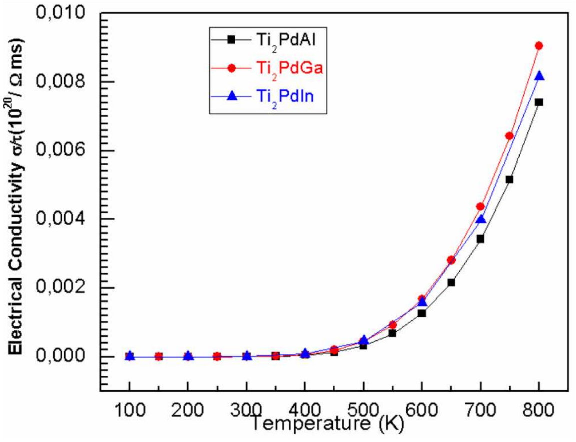

Fig. 12. Calculated Seebeck coefficient of Ti_2PdX as a function of temperature.

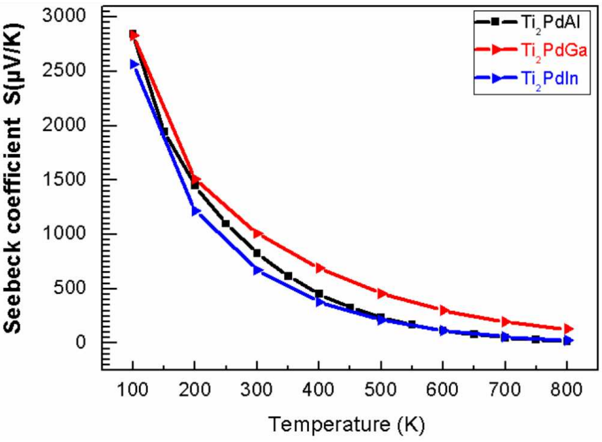

Fig. 13. Calculated electrical conductivity of Ti_2PdX as a function of temperature.

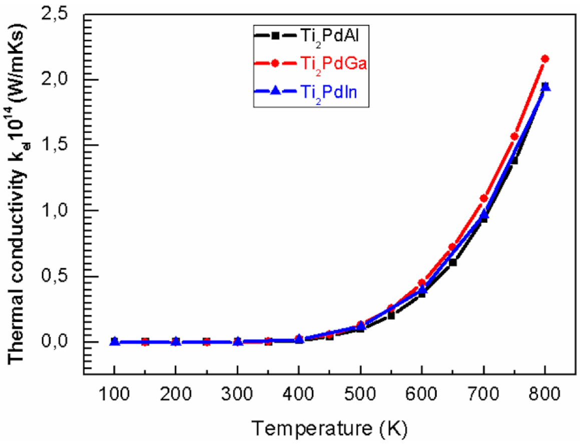

Fig. 14. Calculated thermal conductivity of Ti_2PdX as a function of temperature.

along the whole temperature scale. Thermal conductivities of Ti_2PdX (X = Al, Ga, and In) as a function of chemical potential at 300, 600 and 800 K have been presented in Fig. 11. The electrical conductivities $\sigma(\downarrow)/\tau(\downarrow)$ of the Ti_2PdX compound as a function of temperature, for the spin down, are plotted in Fig. 12, at the Fermi level. The electronic conductivity σ/τ slightly in creases with respect to the temperature down to 300 K. The values of $\sigma(\downarrow)/\tau(\downarrow)$ at room temperature are found to be approximately 0.5427×10^{20}, 1.2284×10^{20}, and 1.7×10^{20} Ω^{-1} m^{-1} S^{-1} for Ti_2PdA1, Ti_2PdGa, and Ti_2PdIn, respectively.

In Fig. 13 at the Fermi level, we notice that the Seebeck coe?cient presents almost the same behavior for the all compounds with maximum values of 2824.38, 2842.65, and 2511.73 μV/K at the temperature of 100 K for the full-Heusler compounds Ti_2PdA1, Ti_2PdGa, and Ti_2PdIn, respectively.

In Fig. 14, we plotted the variation of the electronic thermal conductivity κ/τ with the temperature for the spin-down. We note that κ/τ increases slightly with increase of the temperature and takes the values of 8.30, 11.55, and 15.11 (10^{10} W/(m K)) at room temperature for Ti_2PdAl, Ti_2PdGa, and Ti_2PdIn, respectively.

6. Conclusion

The electronic, magnetic, and thermoelectric properties of Ti_2PdX (X = Al, Ga, and In) have been studied by combining the study of the electronic structures calculated from the first-principle methods with the Boltzmann transport theory. The density of states of paramagnetic and ferromagnetic states, electronic band structures, and total energy calculations clearly suggest the semi-metallic ferromagnetic ground state for these compounds. The band gap is indirect and lies between the points Γ and X, its value is 0.45, 0.50, and 0.45 eV for Ti_2PdA1, Ti_2PdGa, and Ti_2PdIn spin-down semiconductors (SC), respectively. The total magnetic moment obtained from the calculations is 3.00 μ_B per formula unit. The integral value of the magnetic moment confirms the semi-metallic ground state for spin-down. Our study of the thermoelectric is limited to SC spin-down. Our materials can be used in spintronics and thermoelectric fields.

References

[1] F. Heusler, *Verhandl. Deutsch. Physikal. Ges.* **5**, 219 (1903).

[2] M. Bouchard, G. Thomas, *Acta Metall.* **23**, 1485 (1975).

[3] A.A. Knowlton, O.C. Clifford, *Trans. Faraday Soc.* **8**, 195 (1912).

[4] R.M. Bozorth, *Ferromagnetism*, Wiley, 1993, p. 992.

[5] A.J. Bradley, J.W. Rogers, *Proc. R. Soc. A* **144**, 340 (1934).

[6] Y.V. Kudryavtsev, V.A. Oksenenko, *J. Appl. Phys.* **97**, 113903 (2005).

[7] T. Ohoyama, P.J. Webster, R.S. Tebble, *J. Phys. D Appl. Phys.* **1**, 1 (1968).

[8] G.B. Johnston, E.O. Hall, *J. Phys. Chem. Solids* **29**, 193 (1968).

[9] D.P. Oxley, R.S. Tebble, K.C. Williams, *J. Appl. Phys.* **34**, 1362 (1963).

[10] K. Endo, T. Ohoyama, R. Kimura, *J. Phys. Soc. Jpn.* **19**, 1494 (1964).

[11] D.J.W. Geldart, P. Ganguly, *Phys. Rev. B* **1**, 3101 (1970).

[12] A.J. Lapworth, J.P. Jakubovics, *Philos. Mag.* **29**, 253 (1973).

[13] Q. Zeng, I. Baker, J.B. Cui, Z.C. Yan, *J. Magn. Magn. Mater.* **308**, 214 (2007).

[14] J.P. Jakubovics, A.J. Lapworth, T.W. Jolly, *J. Appl. Phys.* **49**, 2002 (1978).

[15] S. Stadler, M. Khan, J. Mitchell, Naushad Ali, *Appl. Phys. Lett.* **88**, 192511 (2006).

[16] C. Guénaut, G. Audi, D. Beck, K. Blaum, G. Bollen, P. Delahaye, F. Herfurth, A. Kellerbauer, H.-J. Kluge, J. Libert, D. Lunney, S. Schwarz, L. Schweikhard, C. Yazidjian, *Phys. Rev. C* **75**, 044303 (2007).

[17] A.J. Muir Wood, C.R. Copcutt, G.Z. Chen, D.J. Fray, *Adv. Eng. Mater.* **5**, 650 (2003).

[18] S.J. Pearton, C.R. Abernathy, M.E. Overberg, G.T. Thaler, D.P. Norton, N. Theodoropoulou, A.F. Hebard, Y.D. Park, F. Ren, J. Kim, L.A. Boatner, *J. Appl. Phys.* **93**, 1 (2003).

[19] P.D. Mitcheson, E.M. Yeatman, G.K. Rao, A.S. Holmes, T.C. Green, *Proc. IEEE* **96**, 1457 (2008).

[20] J.M. Tarascon, M. Armand, in: *Materials for Sustainable Energy*, Ed. V. Dusastre, co-published with Macmillan Publ., UK 2010, p. 171.

[21] D. Jariwala, V.K. Sangwan, L.J. Lauhon, T.J. Marks, M.C. Hersam, *ACS Nano* **8**, 1102 (2014).

[22] A.A. Serga, A.V. Chumak, B. Hillebrands, *J. Phys. D Appl. Phys.* **43**, 264002 (2010).

[23] S.A. Wolf, D.D. Awschalom, R.A. Buhrman, J.M. Daughton, S. Von Molnar, M.L. Roukes, A.Y. Chtchelkanova, D.M. Treger, *Science* **294**, 1488 (2001).

[24] G.A. Prinz, *Science* **282**, 1660 (1998).

[25] C. Chappert, A. Fert, F.N. Van Dau, *Nature Mater.* **6**, 813 (2007).

[26] C.A. Jenkins, Ph.D. thesis, University of California, Berkeley 2009.

[27] N.A. Spaldin, W.E. Pickett, *J. Solid State Chem.* **176**, 615 (2003).

[28] R.L. Stamps, S. Breitkreutz, J. Åkerman, A.V. Chumak, Y. Otani, G.E.W. Bauer, J.-U. Thiele, M. Bowen, S.A. Majetich, M. Kläui, I.L. Prejbeanu, B. Dieny, N.M. Dempsey, B. Hillebrands, *J. Phys. D Appl. Phys.* **47**, 333001 (2014).

[29] M. Bibes, J.E. Villegas, A. Barthelemy, *Adv. Phys.* **60**, 5 (2011).

[30] T. Graf, J. Winterlik, L. Müchler, G.H. Fecher, C. Felser, S. Parkin, in: *Handbook of Magnetic Materials*, Vol. 21, Ed. K.H.J. Buschow, Elsevier, North Holland, 2013, p. 1.

[31] G.K.H. Madsen, D.J. Singh, *Comput. Phys. Commun.* **175**, 67 (2006).

[32] S. Berri, D. Maouche, *J. Supercond. Nov. Magn.* **29**, 2189 (2016).

[33] M. Petersen, F. Wagner, L. Hufnagel, M. Scheffler, P. Blaha, K. Schwarz, *Comput. Phys. Commun.* **3**, 294 (2000).

[34] W. Kohn, L.J. Sham, *Phys. Rev. A* **140**, 1133 (1965).

[35] P. Hohenberg, W. Kohn, *Phys. Rev. B* **136**, 864 (1964).

[36] J.P. Perdew, V.N. Staroverov, J. Tao, G.E. Scuseria, *Phys. Rev. A* **78**, 052513 (2008).

[37] P. Blaha, K. Schwarz, G.K.H. Madsen, D. Kvasnicka, J. Luitz, *WIEN2k: An Augmented Plane Wave Plus Local Orbitals Program for Calculating Crystal Properties*, Vienna University of Technology, Vienna 2001.

[38] H. Gzyl, *J. Stat. Phys.* **29**, 617 (1982).

[39] T.J. Scheidemantel, C. Ambrosch-Draxl, T. Thonhauser, J.V. Badding, J.O. Sofo, *Phys. Rev. B* **68**, 125210 (2003).

[40] G.K.H. Madsen, *J. Am. Chem. Soc.* **128**, 12140 (2006).

[41] S. Fahy, K.J. Chang, S.G. Louie, M.L. Cohen, *Phys. Rev. B* **35**, 5856 (1987).

[42] R.W. Godby, M. Schlüter, L.J. Sham, *Phys. Rev. B* **37**, 10159 (1988).

[43] M. Lannoo, M. Schlüter, L.J. Sham, *Phys. Rev. B* **32**, 3890 (1985).

[44] L. Hedin, B.I. Lundqvist, *Solid State Phys.* **23**, 1 (1969).

[45] F.D. Murnagham, *Proc. Natl. Acad. Sci. USA* **30**, 244 (1944).

[46] J. Wang, S. Yip, S.R. Phillpot, D. Wolf, *Phys. Rev. Lett.* **71**, 4182 (1993).

[47] D.H. Chung, W.R. Buessem, *J. Appl. Phys.* **38**, 2010 (1967).

[48] M. Born, K. Huang, *Dynamical Theory of Crystal Lattices*, Clarendon, Oxford 1956, p. 420.

[49] J.F. Nye, *Physical Properties of Crystals*, Oxford University Press, Oxford 1985.

[50] O. Rabin, L. Yu-Ming, M.S. Dresselhaus, *Appl. Phys. Lett.* **79**, 81 (2001).

[51] T. Takeuchi, *Mater. Trans.* **50**, 2359 (2009).

[52] H.J. Xiang, D.J. Singh, *Phys. Rev. B* **76**, 195111 (2007).

[53] A.S. Botana, P.M. Botta, C. de la Calle, A. Piñeiro, V. Pardo, D. Baldomir, J.A. Alonso, *Phys. Rev. B.* **83**, 184420 (2011).

[54] J. Martin, T. Tritt, C. Uher, *J. Appl. Phys.* **108**, 121101 (2010).

[55] H.C. Kandpal, G.H. Fecher, C. Felser, *J. Phys. D Appl. Phys.* **40**, 1507 (2007).